Cl Nuclear Magnetic Resonance in $CuCl_2 \cdot 2H_2O$*

W. J. O'SULLIVAN
Sandia Laboratory, Albuquerque, New Mexico

AND

W. W. SIMMONS AND W. A. ROBINSON
TRW Space Technology Laboratories, Incorporated, Redondo Beach, California

(Received 28 April 1965; revised manuscript received 19 July 1965)

The ^{35}Cl NMR in single crystals of $CuCl_2 \cdot 2H_2O$ has been studied at 5.0 and 76°K and in the antiferromagnetic state at zero field between 1.3 and 4.2°K. The orientation dependence of the NMR was measured at 5.0°K for fields lying in the *ac* and *bc* crystallographic planes. In addition, the dependence of the NMR frequencies upon applied field strength was measured for particular field orientations. Two possible sets of principal axis systems for the Cl nuclear-site electric field gradient (EFG) and hyperfine field tensors result. This ambiguity is a consequence of the presence of two Cl sites in the unit cell which are distinguishable for general field orientations. However, one set requires that the anisotropic part of the hyperfine field should be dominated by p_π interactions. This is contrary to the expected dominant p_σ contribution for Cu^{++} in $CuCl_2 \cdot 2H_2O$. The second and correct set leads to the hyperfine field values (in units of 10^{-4} cm^{-1}): $A_s = 7.8 \pm 0.6$, $A_\sigma = 5.0 \pm 0.7$, and $A_\pi = 0.0 \pm 0.7$, where we have neglected the second-nearest-neighbor contribution in determining these values. The magnitude of the internal field at a Cl nucleus in $CuCl_2 \cdot 2H_2O$ is 47.5 ± 3.0 kOe at 0°K. The orientation of the EFG is in much better agreement with point-charge-model predictions than with the results of the calculation of Rao and Narasimhamurty in which induced dipole effects were included. The NMR were observed with a superregenerative detector. Since it was not possible to separate the sidebands from the broad central resonance, the resonance patterns consisted of the central resonance with sidebands superimposed. The uncertainty in the location of the central resonance frequencies ($>\pm 15$ kc/sec) proved to be the major source of experimental error. Attempts to observe the resonance with marginal oscillator detectors proved unsuccessful.

I. INTRODUCTION

THE study of transferred hyperfine fields in magnetic insulators has in large part been concentrated upon the iron-group fluorides.[1–5] No comparable effort has developed to investigate transferred hyperfine effects in systems involving larger ligand ions such as Cl^-.

The iron-series chloride and bromide dihydrates ($MX_2 \cdot 2H_2O$, with M=Mn, Fe, Co, Ni, and Cu, and X=Cl or Br) form a group of structurally similar crystalline compounds which undergo transitions to magnetically ordered states. This series of compounds seems to be a promising potential source of information on transferred hyperfine effects in magnetic insulators containing ligand ions larger than F^-. Comparisons between the results of studies of the Cl and Br NMR in different members of this series should provide information of value in spite of the problems associated with the increased number of ligand states.[6]

In this paper we report the results of an investigation of the Cl NMR in $CuCl_2 \cdot 2H_2O$ in both the paramagnetic region and in the antiferromagnetic state. The electric field gradient (EFG) and the hyperfine field at a Cl site in the material are determined. A report of the Cl NMR in $CuCl_2 \cdot 2H_2O$ below the Neél point (T_N) was published[7] before the NMR measurements in the paramagnetic region were begun. The preliminary theoretical fit of the Cl NMR in the antiferromagnetic state proved to be inconsistent with the NMR results in the paramagnetic region. The correct solution is reported in Sec. V of this paper.

II. CRYSTAL STRUCTURE AND SPIN ARRANGEMENT OF $CuCl_2 \cdot 2H_2O$

$CuCl_2 \cdot 2H_2O$ belongs to the orthorhombic system, *Pbmn*, with two formula groups in a unit cell. The

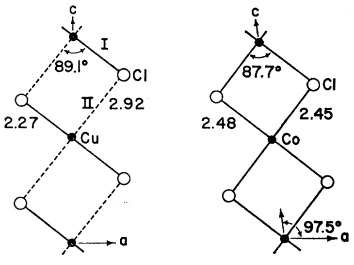

FIG. 1. A segment of a $CuCl_2 \cdot 2H_2O$ chain in $CuCl_2 \cdot 2H_2O$ along with a like segment of a $CoCl_2 \cdot 2H_2O$ chain in $CoCl_2 \cdot 2H_2O$. The bond lengths are in angstroms.

* This work was supported by the U. S. Atomic Energy Commission.

[1] The literature on transferred hyperfine effects in the transition-group fluorides is extensive and we make no effort to assemble a complete list of references on the subject. Most of the experimental work has been done by R. G. Shulman and co-workers at Bell Laboratories. We include a representative selection of their contributions.

[2] R. G. Shulman and V. Jaccarino, Phys. Rev. **108**, 1219 (1957).

[3] R. G. Shulman and K. Knox, Phys. Rev. **119**, 94 (1960).

[4] R. G. Shulman, Phys. Rev. **121**, 125 (1961).

[5] R. G. Shulman and S. Sugano, Phys. Rev. **130**, 506 (1963); K. Knox, R. G. Shulman, and S. Sugano, *ibid.* **130**, 512 (1963); S. Sugano and R. G. Shulman, *ibid.* **130**, 517 (1963).

[6] A. J. Freeman and R. E. Watson, Phys. Rev. Letters **6**, 343 (1961); R. E. Watson and A. J. Freeman, Phys. Rev. **134**, 1526 (1964). These articles contain a rather complete listing of the relevant theoretical and experimental work.

[7] W. J. O'Sullivan, W. W. Simmons, and W. A. Robinson, Phys. Rev. Letters **10**, 475 (1963).

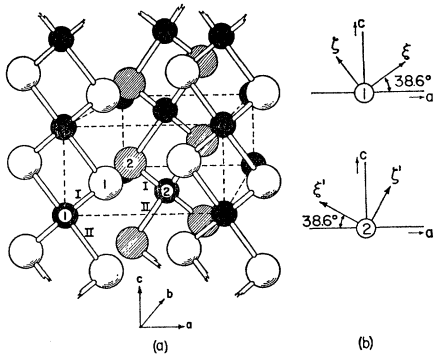

FIG. 2. (a) A unit cell of $CuCl_2 \cdot 2H_2O$ which illustrates the two distinguishable Cu (small circles) and Cl (large circles) sites. Only the Cu and Cl sites are shown as occupied. Since this drawing of the unit cell will be referred to throughout the text it might be of value to emphasize the conventions that will be followed in connection with it. The corner Cu^{++} ion [Cu(1) in the drawing] and the Cl^- ion bonded to it [Cl(1) in the drawing] will be referred to as Cu(1) and Cl(1), respectively. A similar convention will be followed when referring to the second type of Cu and Cl site shown in the drawing. In all cases the numeral I will refer to properties associated with the shorter and II to properties associated with the longer of the two nearest neighbor $Cu^{++}-Cl^-$ bonds. (b) Two coordinate systems which are of importance in this problem. The axes ξ and ζ lie along the bond I axis and its normal in the *ac* plane at a Cl(1) site and the axes ξ' and ζ' lie along the bond I axis and its normal in the *ac* plane at a Cl(2) site.

x-ray analysis of the $CuCl_2 \cdot 2H_2O$ structure was done by Harker.[8] The atomic coordinates, including the proton positions, were later determined with increased accuracy by Peterson and Levy[9] using neutron-diffraction techniques. The dimensions of the orthorhombic unit cell at room temperature are $a=7.38$ Å, $b=8.04$ Å, and $c=3.72$ Å. The structure consists of polymeric $CuCl_2$ chains parallel to the c axis with each Cu^{++} ion surrounded by a distorted square-planar arrangement of Cl^- ions lying in *ac* planes. The distorted nearest-neighbor octahedron about each Cu^{++} ion is completed by the water molecules with the oxygens lying along the b axis on either side of the Cu^{++} ion. In Fig. 1 a segment of a $CuCl_2$ chain in $CuCl_2 \cdot 2H_2O$ is shown along with a like segment of a $CoCl_2$ chain in $CoCl_2 \cdot 2H_2O$. The rhombic arrangement of nearest-neighbor chlorine ions about the copper ions in $CuCl_2 \cdot 2H_2O$ is in contrast to the nearly perfect-square planar array of chlorines about the cobalt ions in $CoCl_2 \cdot 2H_2O$. The longer $Cu^{++}-Cl^-$ bond in $CuCl_2 \cdot 2H_2O$ (bond II in Fig. 1) is approximately 30% longer than the short bond (bond I) and the angle formed by the two bonds is very nearly 90°. The nearest-neighbor M-Cl bonds in the other iron-group chloride dihydrates differ in length by no more than 2%.[10] A $CuCl_2 \cdot 2H_2O$ unit cell is shown in Fig. 2. There are two distinguishable copper sites [Cu(1) and Cu(2) in Fig. 2] and two distinguishable chlorine sites [Cl(1) and Cl(2) in Fig. 2] in the $CuCl_2 \cdot 2H_2O$ lattice. The principal axis systems associated with tensor properties at either the copper or chlorine sites are not completely determined by symmetry. The b axis is a common principal axis for all site tensors. The remaining two principal axes associated with a given site tensor may appear at an arbitrary orientation in the *ac* plane. However, since the two distinct copper or chlorine sites are mirror images of each other in *ab* and *bc* planes, a property tensor at one kind of site is the image of the same property tensor at the second kind of site under reflections in *ab* and *bc* planes.

$CuCl_2 \cdot 2H_2O$ undergoes a transition to a magnetically ordered state at $T_N=4.34$°K. From proton resonance measurements in antiferromagnetic $CuCl_2 \cdot 2H_2O$, Poulis and Hardeman[11] inferred a four sublattice spin arrangement in which the copper spins are arranged antiferromagnetically along the c axes and ferromagnetically in *ab* planes with the sublattice magnetization direction along a. Moriya[12] proposed a model for the $CuCl_2 \cdot 2H_2O$ antiferromagnetic spin arrangement in which the spins are canted slightly ($\simeq 1$°) away from the a axis. Rundle[13] suggested still a third spin structure which is similar to that of Poulis and Hardeman except the spin direction at each face-center site is reversed. Recently, Shirane, Frazer, and Friedberg[14] have carried out a neutron-diffraction experiment on single crystal $CuCl_2 \cdot 2H_2O$ at 1.5°K and have determined that the basic spin structure is that suggested by Poulis and Hardeman. This basic spin arrangement may be canted as proposed by Moriya. However, we are not able to differentiate between a slightly canted structure and the Poulis and Hardeman structure for reasons which are discussed in Sec. V of this paper.

III. EXPERIMENTAL APPARATUS

The magnet used for the chlorine NMR measurements in the paramagnetic region ($T>T_N$) is a Spectromagnetic Industries 4-in. variable gap magnet mounted on a rotating base. A Rawson rotating-coil gaussmeter was used to calibrate the magnetic field as a function of the magnet power-supply helipot reading. By setting the helipot value, the magnetic field at the sample could be reset to within ±20 Oe of a prescribed value after a warmup time of half an hour.

The chlorine nuclear magnetic resonances (NMR) were detected with a superregenerative spectrometer system described in the literature.[15] The resonances were modulated with a sine wave magnetic field at 200 cps with modulation amplitudes ranging from 60–80 Oe rms. In all cases, the NMR were detected at

[8] D. Harker, Z. Krist. **93**, 136 (1936).
[9] S. W. Peterson and H. A. Levy, J. Chem. Phys. **26**, 220 (1957).
[10] B. Morosin and E. J. Graeber, J. Chem. Phys. **42**, 898 (1965).
[11] N. J. Poulis and G. E. G. Hardeman, Physica **18**, 201 (1952).
[12] T. Moriya, Phys. Rev. **120**, 91 (1960).
[13] R. E. Rundle, J. Am. Chem. Soc. **79.3**, 3372 (1957).
[14] G. Shirane, B. C. Frazer and S. A. Friedberg (to be published).
[15] A. Narath, W. J. O'Sullivan, W. A. Robinson, and W. W. Simmons, Rev. Sci. Instr. **35**, 476 (1964).

the second harmonic of the modulation frequency. Since the oscillator frequency during superregenerative operation normally differs by 20–40 kc/sec from that in cw operation, a communications receiver was used to monitor the oscillator frequency as the detector was driven through a resonance.

One single crystal sample of $CuCl_2 \cdot 2H_2O$ was used for all the NMR measurements in the paramagnetic region and a second single crystal was used for the measurements below T_N. The crystals were grown from solution in a constant temperature bath at 23°C. The single crystal samples were roughly 0.1 cm^3 in volume and were needle shaped with the c axis lying along the needle axis.

IV. ELEMENTARY THEORY

In this section we discuss some of the background material concerning the electrostatic and magnetic interactions between nuclei and their environments as it relates to the particular case of Cl nuclei in $CuCl_2 \cdot 2H_2O$.

The important interactions between a Cl nuclear spin and its environment in $CuCl_2 \cdot 2H_2O$ are included in the Hamiltonian,

$$H=\{\mathbf{Q}\}\cdot\{\mathbf{VE}\}-\gamma_N\hbar\mathbf{I}\cdot(\mathbf{H}_0+\mathbf{H}_D) +\mathbf{I}\cdot(\{\mathbf{A}^{\mathrm{I}}\}\cdot\langle\mathbf{S}\rangle^{\mathrm{I}}+\{\mathbf{A}^{\mathrm{II}}\}\cdot\langle\mathbf{S}\rangle^{\mathrm{II}}). \quad (1)$$

The first term in the Hamiltonian represents the coupling between the Cl nuclear quadrupole moment $\{\mathbf{Q}\}$ and the electric field gradient $\{\mathbf{VE}\}$ evaluated at the nucleus (second-rank tensors will be enclosed in curly brackets and principal values of tensors will be labeled with one index, for example, T_i). The second term in Eq. (1) describes the interaction between the magnetic moment of the nucleus and the combination of the applied magnetic field $\mathbf{H}_0$ and the field $\mathbf{H}_D$ at the nucleus due to the magnetic moments on the copper atoms in the lattice. Effects which depend upon the sample shape are included in $\mathbf{H}_D$ for $T>T_N$. Finally, the third term in Eq. (1) characterizes the hyperfine coupling between the Cl nucleus and the magnetic electrons on the two nearest-neighbor copper atoms. The hyperfine tensor is decomposed into two parts, $\{\mathbf{A}^{\mathrm{I}}\}$ which includes only contributions from the interaction between the Cl^- ion and the nearest neighbor Cu^{++} ion (bond I) and $\{\mathbf{A}^{\mathrm{II}}\}$ which is determined by interactions with the second-nearest-neighbor Cu^{++} ion (bond II). The factors $\langle\mathbf{S}\rangle^{\mathrm{I}}$ and $\langle\mathbf{S}\rangle^{\mathrm{II}}$ are the average values of the electron spin on the Cu^{++} ions which are the nearest neighbor and the next-nearest neighbor, respectively, of the chlorine ion. The chlorine NMR data taken below T_N provide hyperfine field information which is distinct from that derived from the NMR in the paramagnetic region. The difference between the bond I and bond II contributions to $\{\mathbf{A}\}$ appears in the internal field below T_N while their sum appears in the internal field above T_N. That is,

$$\langle\mathbf{S}\rangle^{\mathrm{I}}=\langle\mathbf{S}\rangle^{\mathrm{II}}=\langle\mathbf{S}\rangle(T>T_N),$$

and

$$\langle\mathbf{S}\rangle^{\mathrm{I}}=-\langle\mathbf{S}\rangle^{\mathrm{II}}=\langle\mathbf{S}\rangle(T<T_N). \quad (2)$$

If we transform the Hamiltonian to the principal axis system of the EFG (X,Y,Z) and replace the magnetic interactions by a total internal magnetic field at the nucleus, Eq. (1) takes the form,

$$H=A[3I_Z^2-I(I+1)+(\eta/2)(I_+^2+I_-^2)] -\gamma_N\hbar\mathbf{I}\cdot\mathbf{H}_{\mathrm{int}}. \quad (3)$$

In this form of the Hamiltonian, $A=e^2qQ/4I(2I-1)$, Q is the scalar-nuclear-quadrupole moment of the chlorine nucleus, and $eq=eq_Z=(\partial^2V/\partial Z^2)$ is the scalar electric field gradient evaluated at the nucleus $[eq_\alpha=(\partial^2V/\partial\alpha^2)$, where $\alpha=X,Y,Z]$. The asymmetry parameter η characterizes the departure of the EFG from axial symmetry about Z. In all this, the order $|q_Z|>|q_Y|\geqq|q_X|$ has been assumed.

In zero applied field and for $T>T_N$, the eigenvalue spectrum of Eq. (3) consists of two sets of degenerate states $(I=\frac{3}{2})$ separated in energy by an amount,

$$|E_{\pm 3/2}-E_\pm|=6A(1+\eta^2/3)^{1/2}. \quad (4)$$

If rf energy is applied at a frequency corresponding to this energy difference the pure nuclear quadrupole resonance or NQR is observed. The NQR frequency for an $I=\frac{3}{2}$ nucleus is given by,

$$\nu_0=(e^2qQ/2h)(1+\eta^2/3)^{1/2}. \quad (5)$$

That is, $\nu_0=\nu_0(q,\eta)$ if Q is assumed to be known. With a nonzero $\mathbf{H}_{\mathrm{int}}(\theta,\phi)$ [the angle coordinates relate to the coordinate system (X,Y,Z)], the twofold double degeneracy is broken. If $|\mu_N\cdot\mathbf{H}|\ll|e^2qQ|$ a total of five NMR transitions can be observed. In terms of the state labels appropriate at $H_{\mathrm{int}}\cong 0$, the observable transitions are at frequencies given by $\alpha^+=|E_{+3/2}-E_+|/h$, $\alpha^-=|E_{-3/2}-E_-|/h$, $\beta^+=|E_{+3/2}-E_-|/h$, $\beta^-=|E_{-3/2}-E_+|/h$, and $\nu_{+,-}=|E_+-E_-|/h$. For a general field orientation, the resonance pattern exclusive of $\nu_{+,-}$ consists of four frequencies roughly symmetric about the NQR frequency, with one α and β pair lying above ν_0 and the second pair lying below. The observed NMR frequencies are functions of $\mathbf{H}_{\mathrm{int}}(\theta,\phi)$, q and η. We will be concerned only with the α transitions and to a much lesser extent with the β transitions. Values for q, η, and $\mathbf{H}_{\mathrm{int}}(\theta,\phi)$ at a given Cl site can be determined from a fit between the observed NMR patterns and theory, where q, η, and $\mathbf{H}_{\mathrm{int}}(\theta,\phi)$ are parameters to be varied in the calculation. The orientation of the (X,Y,Z) system in the crystal-axis system can be determined from the relation between the NMR patterns and the crystal-axis system.

A fit between theory and the zero-field NMR below T_N leads to values for $|\mathbf{H}_{\mathrm{int}}(T)|$, q, η, and the orientation of the internal field in the (X,Y,Z) system. The orientation of the (X,Y,Z) system relative to the crystallographic system cannot be inferred from the

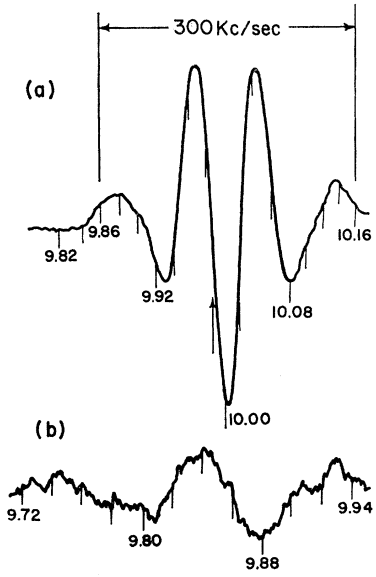

FIG. 3. (a) A ^{35}Cl NMR transition at 5.0°K in an applied field of 1.89 kOe. The arrow marks the approximate location of the resonance center. (b) A ^{35}Cl NMR transition at 76°K in an applied field of 1.89 kOe. The frequency units are megacycles per second and the frequency markers are separated by 20 kc/sec. The quench frequency was 45 kc/sec in both cases.

NMR in the antiferromagnetic state unless an external field is applied.

The unusually large linewidth of the Cl NMR in $CuCl_2 \cdot 2H_2O$ resulted in the NMR measurements in the paramagnetic region being conducted at magnetic fields at which the magnetic interaction could not be considered a simple perturbation upon the electrostatic effects. At temperatures below T_N the situation is reversed. As a result, all experimental NMR frequencies were compared with the exact (computer) solutions of Eq. (3). The general Hamiltonian [Eq. (3)] was programmed for the CDC 1604. The NQR frequency is fed in as input and the output consists of the NMR frequencies and their relative intensities for a given η, and $\mathbf{H}_{\text{int}}(\theta,\phi)$.

Itoh, Fujimoto, and Ibamoto[16] first studied the EPR of Cu^{++} spins in $CuCl_2 \cdot 2H_2O$. Their measurements demonstrated that the copper-ion g tensor represents an average over the two inequivalent copper sites if the Zeeman interaction is smaller than the exchange coupling between neighboring $Cu^{++}(1)$ and $Cu^{++}(2)$ spins. This condition is satisfied throughout the range of magnetic fields applied in our Cl NMR measurements. As a result, the principal axes of the effective Cu^{++} ion g tensor lie along the crystal axes. The Cl-site group in $CuCl_2 \cdot 2H_2O$ (C_{1h}) consists only of the identity plus the mirror operation in the ac plane. Since the ac plane principal axes of both the transferred hyperfine tensor and the lattice dipole sum tensor at a Cl site need not lie along the a and c axes, the hyperfine and dipolar contributions to the internal field may not be describable in terms of real symmetric second-rank tensors. In other words, the loci of the dipolar and hyperfine fields may not have axial symmetry as $\mathbf{H}_0$ is rotated through 360 deg in the ac plane.

[16] J. Itoh, M. Fujimoto, and H. Ibamoto, Phys. Rev. **83**, 852 (1951).

To make the process of extracting internal field information tractable, we *assume* that all of the anisotropic contributions to the internal field can be combined in the field shift tensor, $\{\Delta\mathbf{H}/\mathbf{H}_0\}$, defined as,

$$\mathbf{H}_{\text{int}} = \mathbf{H}_0 + \{\Delta\mathbf{H}/\mathbf{H}_0\} \cdot \mathbf{H}_0, \tag{6}$$

where $\{\Delta\mathbf{H}/\mathbf{H}_0\}$ is a real symmetric second-rank tensor. We will compare the paramagnetic region NMR with calculated results based upon an internal field of the above form. The degree of fit between experiment and theory will be considered as a measure of the validity of using such a simplified representation of the internal field.

V. EXPERIMENTAL RESULTS

A. Paramagnetic Region

The NQR frequencies for chlorine nuclei in $CuCl_2 \cdot 2H_2O$ at 5.0°K are, $\nu_0 = 8.96 \pm 0.02$ Mc/sec (^{35}Cl) and $\nu_0 = 7.04 \pm 0.03$ Mc/sec (^{37}Cl). The NQR frequencies are relatively insensitive to variations in temperature. The ^{35}Cl NQR frequency is 8.98 ± 0.02 Mc/sec at 76°K and 9.01 ± 0.03 Mc/sec at room temperature. The large errors in the quoted resonance frequencies represent reasonable estimates of the possible uncertainty in the location of the resonance center. The width of the Cl NMR in $CuCl_2 \cdot 2H_2O$ is roughly an order of magnitude greater than the width of the Cl NMR in other iron-group chlorides investigated to date. For example, the Cl resonance width in $CoCl_2 \cdot 2H_2O$ is approximately 5 kc/sec,[17] while in $CuCl_2 \cdot 2H_2O$ we estimate the width of the Cl NMR to be $\simeq$50 kc/sec. All attempts to observe either the Cl NQR or NMR in $CuCl_2 \cdot 2H_2O$ with a marginal oscillator detector were unsuccessful. The resonance patterns observed with the superregenerative detector were complicated by the fact that it was not possible to separate the sidebands from the central Cl resonance at quench frequencies as high as 120 kc/sec. The only changes in the resonance pattern (aside from a reduction in signal/noise) for quench frequencies of 100–120 kc/sec was a broadening of the entire pattern. Since we were forced to observe the central resonance in combination with sidebands, the resonance frequency was determined by observing the resonance at various quench frequencies and by locating that portion of the resonance patterns which seemed to be invariant under the change in quench frequency. The success of this recipe for locating the central resonance frequency depends critically upon the signal to noise ratio, but even under the best conditions an uncertainty of $\pm$15 kc/sec represents an optimistic estimate. The relatively large and variable uncertainty in pinpointing the resonance frequencies proved to be the factor which limited the accuracy of our measurements. Two samples of ^{35}Cl NMR patterns at 5.0 and 76°K are shown in Fig. 3. In both cases these NMR correspond to an α transi-

[17] A. Narath (to be published).

tion from one of the two distinguishable Cl sites, under conditions such that the patterns were not influenced by overlapping with another resonance pattern. The reason for including these sample spectra is to give an indication of the better signal-to-noise ratios encountered in this work and to illustrate the complexity of the resonance patterns. The resonance width seems to result from inhomogeneity broadening, rather than from some property of the environment at a given nucleus. At low temperatures (below 2.0°K) the Cl NMR transitions can be saturated. As the rf field level is increased, the central region of the pattern disappears. Then, with an additional increase in the rf intensity, the wings of the pattern disappear. There is no observable variation of the linewidth with temperature from room temperature to 1.3°K. The broadening of the Cl NMR in $CuCl_2 \cdot 2H_2O$ is probably due to effects of strain upon the EFG. However, the resonance width of the NQR in powder samples consisting of microcrystals precipitated from solution was identical within experimental error to the width of the single-crystal patterns. We conclude from this result that even microcrystals of $CuCl_2 \cdot 2H_2O$ are strained. Hence, it is unlikely that one can grow unstrained single crystals of the compound on a macroscopic scale.

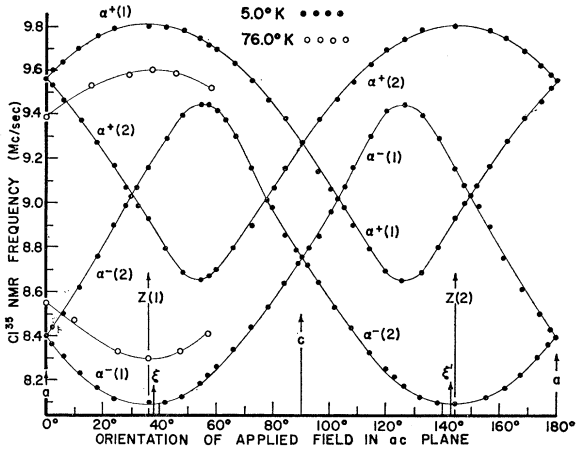

FIG. 4. The ^{35}Cl α transitions in $CuCl_2 \cdot 2H_2O$ at 5.0 and 76°K for a field of 1.6 kOe in the *ac* plane. The resonance frequencies are plotted as a function of the field orientation in the *ac* plane. To make it easier to visualize the relationship between the external field orientation and the Cl-site symmetry we have established a relationship between Fig. 2 and Fig. 4 by assuming that we are rotating the field in Fig. 4 in the *ac* plane through a positive angle away from the *a* axis in Fig. 2. Thus, at 38.6° in Fig. 4 the field is directed along the Cl(1) bond I axis and so on. The other possible relationship between the two figures corresponds to a negative rotation away from the *a* axis in Fig. 2. In this case at 38.6° in Fig. 4 the applied field would be directed along a Cl(2) bond I axis.

Orientation Dependence of the Cl NMR

The first group of NMR experiments consisted of measurements of the ^{35}Cl resonance patterns as a function of the applied field orientation for fields lying in the *ac* and *bc* planes. (Although it is necessary to consider only field orientations in the *ac* plane and along the *b* axis, the *bc* plane data were useful as an additional check of the fit between theory and experiment.) The crystal used in the NMR measurements above T_N was x-ray oriented so that the external field would lie in the respective crystallographic planes to within ±0.5°. The two chlorine sites are equivalent for an applied field in the *bc* plane and only one set of ^{35}Cl and ^{37}Cl NMR transitions were observed. The field was rotated in the *bc* plane through 90° from the *b* axis with intervals of 3° except within the field orientation region where the α^+ and α^- transitions overlap. The *bc* plane resonance pattern was observed at 5.0°K at applied fields of 1.60±0.02 and 3.00±0.02 kOe. The Cl NMR for H_0 in the *ac* plane was studied over a 180° field sweep at 5.0°K and over a limited angular range at 76°K. The measurements were carried out for applied fields of 1.60±0.02 and 3.00±0.02 kOe. The angular interval was 3° except for field orientations near the α transition overlap angles, the *a* and *c* axes, and the EFG principal axes in the *ac* plane. In these sensitive regions the orientation of H_0 was adjusted in increments of from 1° to 0.2°. The ^{35}Cl α transitions observed for a 1.60-kOe field in the *ac* plane at 5.0 and 76°K are plotted in Fig. 4 as a function of the applied field orientation. The double-resonance pattern resulting from the two distinguishable Cl sites is readily apparent. The two sets of transitions are labeled as $\alpha^+(1)$, $\alpha^+(2)$, etc., where (1) and (2) refer to the two Cl sites illustrated in Fig. 2. Since the *b* axis is a principal axis of the Cl EFG tensors, the fact that there are field orientations in the *ac* plane for which $\alpha^+(i) = \alpha^-(i)$ $(i=1,2)$ is proof that the $Z(i)$ axes lie in the *ac* plane. This result is contrary to the prediction by the calculation of Rao and Narasimhamurty[18] that the $Z(i)$ axes lie along *b*. The α overlap orientations could be determined at best to ±1°. The large angular uncertainty is due to two factors. First, the signal/noise ratio for the α transitions in the overlap region is poor, even at 5.0°K. Second, the overlap of the α^+ and α^- patterns, each of which is ≃200 kc/sec wide, is insensitive to field orientation adjustments of less than ±1° about an average orientation which we choose as the overlap angle. The uncertainty in the position of the α overlap angles is not reduced by increasing the field to 3.00 kOe. The β transitions could be observed only with difficulty. At field orientations for which the β intensities are expected to be large, the β transitions from one site are overlapped by the α patterns from the second site. As a result the analysis of our NMR data makes no use of the β transitions.

We see from the data in Fig. 4, that the field orientations corresponding to the maximum frequency difference between the α^+ and α^- transitions are the same within experimental accuracy at 76°K as at 5.0°K.

[18] D. V. G. L. Narasimha Rao and A. Narasimhamurty, Phys. Rev. **132**, 961 (1963).

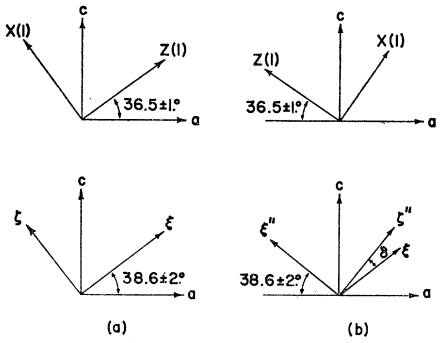

FIG. 5. The two possible orientations of the EFG and field shift principal axis systems at a Cl(1) site: (a) the orientation of the EFG and $\{\Delta H/H_0\}$ principal axis systems that results from the association of the $\alpha(1)$ transition in Fig. 4 with the Cl(1) site in Fig. 2; (b) the orientation of the principal axis systems resulting from the association of the $\alpha(1)$ transition with Cl(2). In (b), the principal axes of $\{\Delta H/H_0\}$ in the ac plane are ξ'' and ζ'', with the maximum principal value of $\{\Delta H/H_0\}$ corresponding to ξ''. The angle δ between ζ'' and the bond I axis (ξ) is $\cong 13°$.

Since a principal axis of the EFG will be close to these directions, and since the field shift at 76°K is reduced from its value at 5.0°K by a factor of approximately $\frac{1}{6}$ (the ratio of the magnetic susceptibilities at 76 and 5.0°K), we conclude that one of two possibilities applies. Either the internal field is isotropic, or the field shift tensor may be anisotropic but its principal axes lie close to the EFG principal axes in the ac plane. The possibility that the contribution of $\{\mathbf{\Delta H/H_0}\}$ to the internal field is small at 5.0°K is excluded by the observed sizable shift between the α transitions at 76 and 5.0°K.

If the internal field at a Cl site were isotropic, the Z axis for a given Cl site would lie along a bisector of one of the angles subtended by the α overlap orientations. This follows, since the locus of the overlap orientations is an elliptical cone about the Z axis which is given by,

$$2\csc^2\theta_0 = 3 - \eta\cos 2\phi_0, \tag{7}$$

where the angles are defined in terms of the (X,Y,Z) system. The α overlap directions we observe in the ac plane would correspond to the intersections of this cone with the ac plane and would be symmetric about the respective Z axes. If we use the observed α overlap orientations the solutions to Eq. (7) are, $Z(1)$ at 36.5 $\pm 1°$, and $Z(2)$ at $142.5\pm 1°$ (the angles correspond to the convention chosen in Fig. 4), $\eta(1)=\eta(2)=0.62$ and $\phi_0=0°$ [$X(1)$ and $X(2)$ lie in the ac plane]. The resultant η for the choice $\phi_0=90°$ is negative. However, the observed α overlap positions in the bc plane are in marked disagreement with the positions predicted using the above selection of parameters. Also, it is not possible to fit the observed ac plane angular pattern with any pattern calculated with an isotropic internal field. We conclude from this result that the internal field has a measurable anisotropy at 5.0°K, and that the principal axes of $\{\mathbf{\Delta H/H_0}\}$ lie close to the EFG principal axes.

Magnetic-Field Dependence of the Cl NMR

Transferred hyperfine effects decrease rapidly as a function of increasing separation between the paramagnetic ion and the anion. Since the relative difference between the bond I and bond II lengths is very large ($\simeq 30\%$ in $CuCl_2\cdot 2H_2O$) we expect that the principal axis of $\{\mathbf{\Delta H/H_0}\}$ corresponding to its largest principal element should lie close to the bond I direction. The fact that the maximum value of the difference between the α transitions at 5.0 and 76°K seems to be in the neighborhood of a bond I direction is evidence that this may be realized.

The second type of experiment consisted of measurements of the shift of the $\alpha^+(1)$ transition (see Fig. 4) as a function of applied field strength for H_0 along ξ, ζ, and b. The ξ and ζ axes lie along the bond I(1) axis and its normal in the ac plane, respectively (see Fig. 2). [The equivalent set of axes for a Cl(2) site is labeled ξ', ζ', and b.] The measured $\alpha^+(1)$ frequency was plotted as a function of the magnitude of H_0 along these three directions and compared with a series of plots of the calculated $\alpha^+(1)$ frequency as a function of the magnitude of $H_{\rm int}$ for various values of η. In the first approximation, $Z(1)$ was chosen to lie along 36.5° in Fig. 4 (the isotropic field solution). The asymmetry parameter was varied from 0.10 to 0.70 in increments of 0.05. The elements $(\Delta H/H_0)_i (i=\xi,\zeta,b)$ for a particular value of η were determined by subtracting the value of $H_{0,i}$ corresponding to a given value of $\alpha^+(1)$ from the value of $H_{{\rm int},i}$ corresponding to an equal calculated frequency and dividing by $H_{0,i}$. That is

$$(\Delta H/H_0)_i = (H_{{\rm int},i}(\eta) - H_{0,i})/H_{0,i},$$

where

$$\alpha_{\rm calc}{}^+(1) = \alpha^+(1). \tag{8}$$

This process was repeated for a series of values of H_0 from 1.0 to 3.0 kOe and the results for each orientation were averaged. The spread of $(\Delta H/H_0)_i$ values for a given η over the range of H_0 was always less than the estimated experimental error. Theoretical fits to the α transition angular plots were attempted as a function of η and the corresponding $(\Delta H/H_0)_i$ under the assumption that the principal axes of $\{\mathbf{\Delta H/H_0}\}$ lie along ξ, ζ, and b. In each case, the first step in the attempted fit involved adjusting the orientation of the Z axis to account for the slight departure from collinearity of H_0 and $H_{\rm int}$ for H_0 oriented a few degrees from ξ. However, the maximum variation of the orientation of Z from the uniform field prediction was $\simeq 1°$. Since the error in the orientation of Z is at least $\pm 1°$, this effect is negligible.

The ac plane and bc plane NMR data at 1.6 and 3.0 kOe were fitted to within experimental error over the entire range of applied field orientations for, $Z(1)$ at $36.5\pm 1°$, $X(1)$ at $126.5\pm 1°$, and $Y(1)$ along b (the angles are with reference to Fig. 4). The value of the asymmetry parameter is $\eta = 0.42\pm 0.07$ and the values

of the field shift at 5.0°K are, $(\Delta H/H_0)_\xi = 0.34 \pm 0.02$, $(\Delta H/H_0)_\zeta = 0.06 \pm 0.02$, and $(\Delta H/H_0)_b = 0.05 \pm 0.02$.

One additional set of measurements was carried out. The frequency shift of the $\alpha^+(1)$ transition was studied as a function of applied field strength at 5.0°K for field orientations in an angular range of $\pm 10°$ about the ξ direction with increments of 1°. It was assumed in each case that H_0 was directed along a principal axis of $\{\Delta\mathbf{H}/\mathbf{H}_0\}$. The elements of $\{\Delta\mathbf{H}/\mathbf{H}_0\}$ were determined as functions of η for the field direction and its normal in the *ac* plane. Theoretical fits to the *ac*-plane NMR data were attempted for each $\mathbf{H}_0$ orientation. For $\mathbf{H}_0$ at more than $\pm 2°$ from ξ the fit over the entire angular range was poorer and for $\mathbf{H}_0$ at more than $\pm 3°$ from ξ the fit was outside the experimental limits.

We conclude that the principal axes of the field-shift tensor and the electric-field-gradient tensor at a Cl(1) position in $CuCl_2 \cdot 2H_2O$ are oriented as shown in Fig. 5(a). The asymmetry parameter at either Cl site is equal to 0.42 ± 0.07. The estimated error in the orientation of the Z and X axes is $\pm 1°$ and the estimated error in the orientation of principal axes of $\{\Delta H/H_0\}$ in the *ac* plane is $\pm 2°$. The elements of the field-shift tensor at a Cl(1) and Cl(2) site at 5.0°K are, respectively,

$$(\Delta H/H_0)_\xi = (\Delta H/H_0)_{\xi'} = 0.34 \pm 0.02,$$
$$(\Delta H/H_0)_\zeta = (\Delta H/H_0)_{\xi'} = 0.06 \pm 0.02,$$

and,

$$(\Delta H/H_0)_b = 0.05 \pm 0.02. \quad (9)$$

The assumption has been implicit throughout the preceding discussion that the $\alpha(1)$ transitions are in fact associated with the Cl(1) site and that the $\alpha(2)$ transitions are associated with Cl(2) site. However, the association of a given site to a particular Cl resonance pattern in $CuCl_2 \cdot 2H_2O$ cannot be made without the application of physical arguments. The alternative possible arrangements of the principal axes of the EFG tensor and field-shift tensor at a Cl(1) site are illustrated in Fig. 5(b).

The two possible sets of principal axis systems at a Cl(1) site will be referred to as case (a) and case (b) corresponding to Fig. 5(a) and (b), respectively. The evidence in favor of case (a) is strong. We will carry out the subsequent analysis of the experimental results under the assumption that case (a) applies. The arguments against case (b) will be summarized at the end of Sec. VII.

B. Cl NMR in the Antiferromagnetic State

The ^{35}Cl and ^{37}Cl NMR transitions in $CuCl_2 \cdot 2H_2O$ were detected in zero applied field from 1.2 to 4.25°K. The NMR measurements below T_N were reported in an earlier publication.[7] A rough analysis of that data resulted in a solution which gave an apparent fit to within ± 250 kc/sec of the observed frequencies over the temperature range $1.35°K \leq T \leq 3.5°K$. However, this solution was inconsistent with our results for the NMR at 5.0°K.

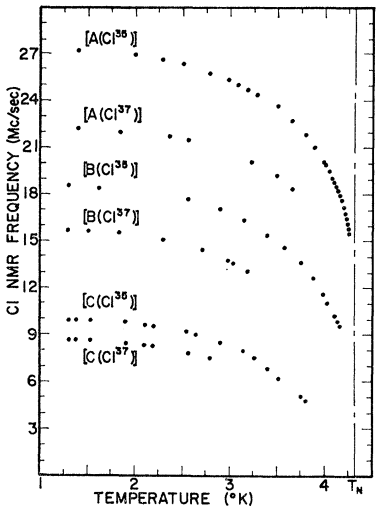

FIG. 6. The ^{35}Cl and ^{37}Cl zero-field NMR transitions in antiferromagnetic $CuCl_2 \cdot 2H_2O$. The observed resonances correspond to the following transitions: (A) $[-\frac{3}{2} \leftrightarrow -\frac{1}{2}]$, (B) $[-\frac{1}{2} \leftrightarrow +\frac{1}{2}]$, and (C) $[\frac{3}{2} \leftrightarrow \frac{1}{2}]$, where the state labels are those which are valid in the high-field limit and where we have assumed that e^2qQ is negative.

The Cl NMR below T_N were remeasured in zero field from 1.3 to 4.10°K. The uncertainty in the location of the resonance frequencies was reduced from ± 50 to ± 15 kc/sec by using a communication receiver to monitor the oscillator frequency during superregenerative operation. (The Cl NMR data are plotted as a function of temperature in Fig. 6.) The experimental NMR frequencies were then compared with the calculated frequencies determined from the computer solutions of Eq. (3). The adjustable parameters were $|\mathbf{H}_{\text{int}}|$, η, θ, and ϕ. The latter two parameters are the angular coordinates of the internal magnetic field in the EFG principal axis system. The NMR data were fitted to within ± 20 kc/sec over the total temperature range (1.3–4.1°K) with the selection of parameters: $|\mathbf{H}_{\text{int}}(T=0°K)| = 47.5 \pm 3.0$ kOe, $\eta = 0.45 \pm 0.05$, $\theta = \pm(4° \pm 1°)$ and $\phi = 0°$ (X axis in the *ac* plane). The error limits in the quoted magnitude of the internal field at 0°K represent an estimate of the error involved in extrapolating the observed NMR frequencies to 0°K. The fit between experiment and theory is insensitive to small variations in θ and η. This fact, coupled with the large error limits associated with the paramagnetic region results rule out any possibility of our discriminating between the Moriya[12] and Poulis and Hardeman[11] spin structures.

A single attempt was made to detect the Cl NMR below T_N in an applied field. We were not able to observe a resolved resonance pattern with a field of 4 kOe oriented along various directions in the *ac* plane.

It is known from the proton resonance measure-

ments[11] in antiferromagnetic $CuCl_2 \cdot 2H_2O$ that the sublattice magnetization directions either lie along or very close to the a axis. The fact that the internal field at a Cl nucleus in antiferromagnetic $CuCl_2 \cdot 2H_2O$ is oriented at $\pm 4°$ from the Z axis of the EFG [i.e., at 32.5° or 40.5° from a in Fig. 4 at a Cl(1) site] is striking evidence of the anisotropy of the hyperfine field.

From their measurements of the zero-field proton NMR in antiferromagnetic $CuCl_2 \cdot 2H_2O$, Poulis, *et al.*[19] determined that the internal field at a proton varied as T^4 over a temperature range from 0.9°K to nearly 4°K. We compared $\ln[H_{\text{int}}(0) - H_{\text{int}}(T)]$ for a Cl nucleus against $4 \ln T$ for temperatures between 1.3 and 4.0°K. The fit of our data to a T^4 law is not as apparent as in the proton case. Since the error involved in the extrapolation of $H_{\text{int}}(T)$ to 0°K is large, the comparison is of particularly doubtful significance within the lower part of the temperature range. To eliminate the extrapolation error and to check the possibility that the temperature dependence of the field at the Cl nuclei differs from that at the protons, we compared $H_{\text{int}}(T)$ at a Cl nucleus with $H_{\text{int}}(T)$ at a proton, where the latter values were determined from the zero-field proton-resonance data.[19] We find that the temperature dependence of the field at a Cl nucleus and at a proton are identical to within experimental error over the temperature range within which the comparison could be made (1.3 to 3.9°K). Hence, while we cannot offer a meaningful check of the T^4 magnetization behavior, we can say that the temperature dependence of the field at the Cl nuclei and the protons in antiferromagnetic $CuCl_2 \cdot 2H_2O$ agree within the accuracy of our measurements.

VI. EFG AT A Cl SITE IN $CuCl_2 \cdot 2H_2O$

The value of the crystal-field description of the electrostatic environment of ions in crystals has been well established in those cases where the coefficients appearing in the expansion of the model potential are determined from experiment. It is possible to calculate the potential for particular models of the crystal field from first principles. However, the value of the results of such calculations as representations of the electrostatic fields in crystals is questionable.

The comparison between the EFG determined from experiment and the EFG calculated from some model of the crystal field provides one test of the calculated potential. If the electric quadrupole moment of the nucleus is known, the principal values of the EFG tensor are directly related to the second multipole moment of the charge distribution external to the nucleus.[20] As a result, the experimental values for the EFG at nuclei in solids can be used to test that part of a model charge distribution which transforms under rotations as the second order spherical harmonics.

The point-charge approximation represents the most elementary model of the crystal field in ionic solids. In this model all ions external to a given atom are replaced by point charges at the lattice sites. In the context of this model, the EFG at the kth nucleus is given by,

$$eq_{\text{ionic}} = 2\left[(1-\gamma_\infty) \sum_{i \neq k} e_i \frac{P_2(\cos\theta_i)}{r_i^3} + \int_{\text{atom } k} \frac{\rho(r) P_2(\cos\theta) d^3r}{r^3} \right], \tag{10}$$
$$= eq_{\text{lattice}} + eq_{\text{atom}}.$$

The first term in Eq. (10) is the contribution of the lattice of point charges to the EFG. The second term represents that part of the EFG due to the electronic charge distribution of the kth atom. The factor $(1-\gamma_\infty)$ in the lattice contribution is the antishielding constant. This factor accounts for the effect upon the EFG of the distortion of the kth-atom-charge distribution caused by the external charges.

This model provides values of q_{ionic} which are in reasonable agreement with experiment for the case of positive ion nuclei in ionic lattices, where both the antishielding factors and q_{atom} are small. In general, the point charge model has failed to provide more than a qualitative description of the EFG at negative ion nuclei in ionic solids. The negative ion valence electrons extend further out into the lattice than the more tightly bound positive ion valence electrons. Thus, the EFG at negative ion nuclei are characterized by the increased importance of antishielding effects (large γ_∞) and the effects of overlapping between the neighboring valence-electron distributions.

Recently, attempts have been made to modify the elementary ionic model by including contributions due to induced electric-dipole moments at the lattice points in addition to the point-charge contribution. It is observed in all cases investigated[18,21] that the crystal-field coefficients are substantially influenced by the inclusion of induced dipoles. The crystal-field model, even when subjected to more sophisticated modifications[22–24] has proved unsuccessful in predicting the values of the observed Stark splittings in crystals. Therefore, one must question whether the introduction of induced dipole effects represents an improvement over the point-charge model despite the evident large induced dipole contribution to the crystal-field potential.

Rao and Narasimhamurty[18] (R and N) calculated both the EFG at a Cl nucleus and the crystal axis components of the g tensor for a Cu^{++} ion, in $CuCl_2 \cdot 2H_2O$. The calculations were first carried out for the point-charge representation of the lattice with the

[19] N. J. Poulis, G. E. G. Hardeman, W. Van Der Lugt, and W. P. A. Hass, Physica **24**, 280 (1958).
[20] A. Abragam, *The Principles of Nuclear Magnetism* (Oxford University Press, London, England, 1961), Chap. VI.
[21] R. R. Sharma and T. P. Das, J. Chem. Phys. **41**, 3581 (1964).
[22] W. H. Kleiner, J. Chem. Phys. **20**, 1784 (1952).
[23] J. C. Phillips, J. Phys. Chem. Solids **11**, 26 (1959).
[24] A. J. Freeman and R. E. Watson, Phys. Rev. **120**, 1254 (1960).

TABLE I. Principal values of the EFG tensor at a Cl site in $CuCl_2 \cdot 2H_2O$. The experimental value is for an assumed $\gamma_\infty = -27$ and a NQR frequency of 8.96 Mc/sec. The sign of the experimental q_Z is arbitrary. The orientations of the principal axes are given in terms of the direction cosines with respect to the a, b, and c crystal axes, respectively.

	R and N (Point charge)	R and N (Induced dipoles)	This paper (Point charge)	Experiment
q_Z(Å^{-3})	0.1189 (±0.782, 0, ±0.623)	−0.0736 (0,1,0)	0.17715 (±0.843, 0, ±0.537)	0.225 (±0.803, 0, ±0.595)
q_Y(Å^{-3})	−0.0741 (0,1,0)	0.0634 (±0.975, 0, ±0.223)	−0.15428 (0,1,0)	−0.160 (0,1,0)
q_X(Å^{-3})	−0.0447 (∓0.623, 0, ±0.782)	0.0104 (∓0.223, 0, ±0.975)	−0.02287 (∓0.537, 0, ±0.843)	−0.065 (∓0.595, 0, ±0.803)
$\eta=(q_X-q_Y)/q_Z$	0.25	0.72	0.74	0.42

water molecules replaced by their estimated permanent dipole moment. Then the model was adjusted to include the effects of induced dipole moments located on the chlorine and oxygen sites in the lattice. The results of their calculations of the Cl site EFG are included in Table I along with the results of an independent point-charge-model calculation of the EFG. The latter calculation was carried out using a lattice sum routine programmed for the CDC 1604 by A. Narath. The program has been tested thoroughly and results are considered accurate to ±0.1%. The discrepancy between the results of the two point-charge calculations can probably be understood as follows. The atomic positions (including the proton locations) determined by the neutron diffraction measurements of Peterson and Levy[9] were used in our calculation. Rao and Narasimhamurty used estimated Cl-O and Cl-Cu distances which are larger by approximately 5% than the Peterson and Levy values. Nevertheless, the two-point charge estimates of the field gradient agree reasonably well with regard to the orientation of the field-gradient principal axis system.

If we compare the experimental NQR frequency with the NQR frequencies predicted on the basis of the above calculations, we find for a ^{35}Cl nucleus,

$(e^2q_{\text{calc}}Q/2h)(1-\gamma_\infty)$

$=7.4$ Mc/sec (our calculation)

$=4.8$ Mc/sec (R and N point charge)

$=3.1$ Mc/sec (R and N point charge plus induced dipoles),

and

$$(e^2q_{\text{exptl}}Q/2h)=8.96 \text{ Mc/sec } (5.0^\circ\text{K}), \qquad (11)$$

where we use the value $\gamma_\infty=-27$ as estimated by Burns and Wikner[25] for ^{35}Cl. No conclusions can be drawn from this comparison, particularly since the two point-charge-model values differ widely. However, experience with ionic-model calculations in other paramagnetic chlorides[17,26] such as $CoCl_2 \cdot 2H_2O$ and $CrCl_3$ suggests that while the point-charge-model principal values are of little significance, the model does provide a reasonable prediction of the orientation of the EFG principal axes. From Table I we see that both point-charge calculations predict principal axis orientations which agree quite well with the experimental orientation. On the other hand, the inclusion of induced dipole effects leads to an EFG orientation in marked disagreement with the experimental results.

Rao and Narasimhamurty calculated the elements of the Cu^{++} g tensor using the same models of the crystal field they applied to the EFG calculation. They found that with the simple point-charge description of the crystal field the calculated g values differed by as much as 50% from the experimental values. However, with the addition of the induced dipole contribution to the potential they were able to calculate g values agreeing with the experimental values to within 0.5%.

Since Rao and Narasimhamurty employed the same model of the crystal field to determine both the Cl site EFG and the Cu^{++} g tensor values, it would seem that the extremely good agreement they find for the g values is fortuitous and, in this case, the addition of the induced dipole contributions probably does not represent an improvement upon the point-charge model.

VII. DETERMINATION OF THE ELEMENTS OF $\{A\}$

A. Case (a)

The magnetic field at a chlorine nucleus due to magnetic-dipole contributions was calculated using a dipole sum routine programmed for the CDC 1604 by A. Narath. An isotropic magnetic moment equal to $2\mu_B$ was assumed for the Cu^{++} ions. The dipole sum was taken over a 200 Å radius sphere within the $CuCl_2 \cdot 2H_2O$ lattice. The number of lattice points in the sum was sufficient to ensure an accuracy of 0.1% in the calculated values. The dipole contribution was smaller than the experimental error in the total field at a Cl nucleus both in the paramagnetic region and below T_N. For example, the dipole field at a Cl nucleus at 0°K is $\simeq$1.65 kOe for a completely aligned Poulis and Hardeman[12] structure. Since the dipolar contribu-

[25] G. Burns and E. G. Wikner, Phys. Rev. **121**, 155 (1961).
[26] B. Morosin and A. Narath, J. Chem. Phys. **40**, (1965) 1958.

tion to the field at a Cl nucleus is less than the experimental uncertainty in $\mathbf{H}_{\text{int}}$, the internal field derivable from the Cl NMR studies is determined solely by the hyperfine contributions.

The paramagnetic region NMR data have been shown to be consistent with an $\mathbf{H}_{\text{int}}$ written in terms of a real symmetric tensor, $\{\Delta\mathbf{H}/\mathbf{H}_0\}$, whose principal axes in the *ac* plane are rotated relative to the crystal axes. This result indicates that our NMR measurements are not accurate enough to detect effects due to the small anisotropy of the Cu^{++} g tensor in the *ac* plane $[(g_c-g_a)/g_c\cong 0.03]$. Therefore, we neglect off diagonal contributions and take the components of the Cu^{++} ion g tensor and the paramagnetic susceptibility tensor along the principal axes of $\{\Delta H/H_0\}$. That is, $g_\xi=g_{\xi'}=2.21$, $g_\eta=g_{\eta'}=2.23$, and $g_b=2.03$, where we have used the experimental values[27] $g_a=2.19$, $g_c=2.25$, and $g_b=2.03$. Similarly, we use the result of the susceptibility measurements of Van Der Marel *et al.*[28] to find (units are 10^{-2}/mole) $\chi_\xi=\chi_{\xi'}=3.27$, $\chi_\eta=\chi_{\eta'}=3.32$, and $\chi_b=2.85$, for the paramagnetic susceptibilities along the principal axes of $\{\Delta\mathbf{H}/\mathbf{H}_0\}$ at 5.0°K. In this approximation, the average value of the Cu^{++} ion spin along the ith principal axis of $\{\Delta\mathbf{H}/\mathbf{H}_0\}$ is given by,

$$\langle S\rangle_i=-(\chi_i-\chi_i^0)H_{0,i}/Ng_i\mu_B. \tag{12}$$

In Eq. (12) $\mathbf{S}$ corresponds to the fictitious spin appearing in the spin Hamiltonian for a Cu^{++} ion in the $CuCl_2\cdot 2H_2O$ lattice and χ_i^0 is the temperature-independent contribution to the susceptibility. (In the case of Cu^{++} the fictitious spin and the true spin are both equal to $\frac{1}{2}$.) This expression for the average spin components is valid at temperatures close to the antiferromagnetic transition temperature if the susceptibility remains a smoothly varying function of temperature and if the onset of long-range spin order is delayed until the transition temperature is reached. The temperature independent contribution to the paramagnetic susceptibility is negligible (we use a spin-orbit coupling parameter of -600 cm^{-1} inferred from the results of Abragham and Price[29] in the Cu Tutton salts to arrive at this conclusion) and the expression for the average spin components is simply,

$$\langle S\rangle_i=-(\chi_i/g_i)H_{0,i}/N\mu_B. \tag{13}$$

If we combine the corresponding values of χ_i and g_i in Eq. (13), the average spin components at 5.0°K are,

$$\langle S\rangle_\xi/H_{0,\xi}=\langle S\rangle_{\xi'}/H_{0,\xi}=-2.65\times 10^{-6}\ \text{Oe}^{-1},$$
$$\langle S\rangle_\eta/H_{0,\eta}=\langle S\rangle_{\eta'}/H_{0,\eta'}=-2.66\times 10^{-6}\ \text{Oe}^{-1},$$

and

$$\langle S\rangle_b/H_{0,b}=-2.51\times 10^{-6}\ \text{Oe}^{-1}. \tag{14}$$

Since $\langle S\rangle_\xi$ and $\langle S\rangle_\eta$ are equal to within the accuracy of the susceptibility values, we assume that $\{\langle\mathbf{S}\rangle/\mathbf{H}_0\}$ is isotropic in the *ac* plane with a value given by, $\langle\bar{S}\rangle/H_0=-2.65\times 10^{-6}$ Oe^{-1}.

The relation between the principal values of the field-shift tensor and the transferred hyperfine tensor at a Cl nucleus in the paramagnetic region is,[30]

$$(\Delta H/H_0)_i=(A^{\text{I}}+A^{\text{II}})_i\langle S\rangle_i/\gamma_N\hbar H_{0,i}. \tag{15}$$

The resulting principal values at a Cl(1) site at 5.0°K are

$$(\gamma_N\hbar)^{-1}(A^{\text{I}}+A^{\text{II}})_\xi=128\pm 8\ \text{kOe},$$
$$(\gamma_N\hbar)^{-1}(A^{\text{I}}+A^{\text{II}})_\zeta=20\pm 8\ \text{kOe},$$

and

$$(\gamma_N\hbar)^{-1}(A^{\text{I}}+A^{\text{II}})_b=20\pm 8\ \text{kOe}. \tag{16}$$

A fourth independent combination of the hyperfine parameters can be extracted from the NMR in the antiferromagnetic region. The internal field components at a Cl nucleus at 0°K with $H_0=0$ and $H_D=0$ are

$$H_{\text{int},i}=(\gamma_N\hbar)^{-1}(A^{\text{I}}-A^{\text{II}})_i\beta S_i, \tag{17}$$

where β is the degree of alignment of the magnetic sublattices at 0°K and $|\mathbf{S}|=\frac{1}{2}$. The internal field extrapolated to 0°K is 47.5±3.0 kOe. The field at a Cl(1) nucleus lies in the *ac* plane at $\theta_{\text{int}}\cong 32°$ or 40° with respect to the *a* axis (the angle convention is that chosen in Fig. 4). We assume that $\mathbf{S}$ is directed along the *a* axis and equate the components of the internal field along ξ and ζ from Eq. (17) to the experimental internal field components along ξ and ζ (extrapolated to 0°K). The combinations of hyperfine field parameters below the Neél point are

$$(\gamma_N\hbar)^{-1}(A^{\text{I}}-A^{\text{II}})_\xi=\pm(121\pm 8\ \text{kOe})/\beta$$

and

$$(\gamma_N\hbar)^{-1}(A^{\text{I}}-A^{\text{II}})_\zeta=\pm(16\pm 4\ \text{kOe})/\beta$$
$$\text{or}\ \mp(5\pm 4\ \text{kOe})/\beta. \tag{18}$$

The two values for $(A^{\text{I}}-A^{\text{II}})_\zeta$ correspond to $\theta_{\text{int}}\cong 32°$ and 40°, respectively. The *b* axis component of the hyperfine parameters is not involved in the zero-field NMR below T_N since the internal field lies in the *ac* plane. The uncertainty in the sign of the values in Eq. (19) results from our inability to distinguish between the two possible senses of $\mathbf{H}_{\text{int}}$. If we set[31] $\beta=0.95$ and transform the result from kOe to cm^{-1}, the hyperfine components for a ^{35}Cl(1) nucleus in $CuCl_2\cdot 2H_2O$ are (units are 10^{-4} cm^{-1}),

$$(A^{\text{I}}+A^{\text{II}})_\xi=17.7\pm 1.0,$$
$$(A^{\text{I}}+A^{\text{II}})_\zeta=2.8\pm 1.0,$$
$$(A^{\text{I}}+A^{\text{II}})_b=2.8\pm 1.0,$$
$$(A^{\text{I}}-A^{\text{II}})_\xi=\pm 17.7\pm 1.2,$$

[27] H. J. Gerritsen, R. Okkes, B. Bölger, and C. J. Gorter, Physica **21**, 629 (1955).

[28] L. C. Van Der Marel, J. Van Den Broek, J. D. Wasscher, and C. J. Gorter, Physica **21**, 685 (1955).

[29] A. Abragam and M. H. L. Pryce, Proc. Roy. Soc. (London) **A205**, 164 (1950).

[30] J. W. Stout and R. G. Shulman, Phys. Rev. **118**, 1136 (1960).

[31] The value chosen for the degree of sublattice alignment ($\beta=0.95$) represents a convenient guess, rather than an estimate. A variation of β through the range 0.90–1.00 introduces no significant change in our numerical results.

and

$$(A^{\mathrm{I}}-A^{\mathrm{II}})_{\zeta}=\pm 2.1\pm 0.7(\mp 0.7\pm 0.7). \quad (19)$$

The second numerical value for $(A^{\mathrm{I}}-A^{\mathrm{II}})_{\zeta}$ corresponds to $\theta_{\mathrm{int}}\cong 40°$ (this convention will be followed throughout the remainder of the section). The assigned error limits are estimated experimental errors.

The hyperfine interaction at a Cl nucleus in $CuCl_2\cdot 2H_2O$ can be written as[32]

$$A_i{}^N=A_s{}^N+A_\sigma{}^N(3\cos^2\theta_{i,\sigma}-1)+A_\pi{}^N(3\cos^2\theta_{i,\pi}-1), \quad (20)$$

where the index i runs over the three principal axes of the hyperfine tensor and $N=$ I or II for the type I or type II bonds. The total isotropic interaction $(A_s{}^{\mathrm{I}}+A_s{}^{\mathrm{II}})$ is associated with the unpaired s electron spin density at the Cl nucleus.

As shown by Tinkham,[32] the anisotropic part of the hyperfine interaction is a measure of the difference of the spin density associated with two of the p orbitals from that of the third orthogonal one. We choose the P_σ orbitals directed along the respective Cu^{++}-Cl^- bonds as one of the two and the p_π orbitals directed along the b axis as the other. The third orbital, which Tinkham calls the $p_{\pi'}$ orbital will be normal to the respective bond in the ac plane. In Tinkham's notation, $A_\sigma{}^N$ and $A_\pi{}^N$ are shorthand for $A_\sigma{}^N-A_{\pi'}{}^N$ and $A_\pi{}^N-A_{\pi'}{}^N$, respectively. The angles $\theta_{i,\sigma}$ and $\theta_{i,\pi}$ are the angles between the p_σ and p_π axes and the magnetic field.

The total s electron contribution to the hyperfine interaction can be determined from Eq. (20). This is,

$$A_s{}^{\mathrm{I}}+A_s{}^{\mathrm{II}}=\tfrac{1}{3}\textstyle\sum_i (A^{\mathrm{I}}+A^{\mathrm{II}})_i = 7.8\pm 0.6\times 10^{-4}\ \mathrm{cm}^{-1}, \quad (21)$$

for a ^{35}Cl nucleus in $CuCl_2\cdot 2H_2O$. In addition we are able to derive some information regarding the anisotropic part of the hyperfine interaction. If we write out the combinations of factors in Eq. (20) which correspond to the hyperfine components in Eq. (19), the following relations result [we have approximated the angle between the bond I and bond II directions (89.1°) by 90°]:

$$(A^{\mathrm{I}}+A^{\mathrm{II}})_{\xi}=A_s{}^{\mathrm{I}}+A_s{}^{\mathrm{II}}+2A_\sigma{}^{\mathrm{I}}-A_\sigma{}^{\mathrm{II}}-A_\pi{}^{\mathrm{I}}-A_\pi{}^{\mathrm{II}},$$
$$(A^{\mathrm{I}}+A^{\mathrm{II}})_{\zeta}=A_s{}^{\mathrm{I}}+A_s{}^{\mathrm{II}}-A_\sigma{}^{\mathrm{I}}+2A_\sigma{}^{\mathrm{II}}-A_\pi{}^{\mathrm{I}}-A_\pi{}^{\mathrm{II}},$$
$$(A^{\mathrm{I}}+A^{\mathrm{II}})_{b}=A_s{}^{\mathrm{I}}+A_s{}^{\mathrm{II}}-A_\sigma{}^{\mathrm{I}}-A_\sigma{}^{\mathrm{II}}+2(A_\pi{}^{\mathrm{I}}+A_\pi{}^{\mathrm{II}}),$$
$$(A^{\mathrm{I}}-A^{\mathrm{II}})_{\xi}=A_s{}^{\mathrm{I}}+A_s{}^{\mathrm{II}}+2A_\sigma{}^{\mathrm{I}}+A_\sigma{}^{\mathrm{II}}-A_\pi{}^{\mathrm{I}}+A_\pi{}^{\mathrm{II}},$$

and,

$$(A^{\mathrm{I}}-A^{\mathrm{II}})_{\zeta}=A_s{}^{\mathrm{I}}-A_s{}^{\mathrm{II}}-A_\sigma{}^{\mathrm{I}}-2A_\sigma{}^{\mathrm{II}}-A_\pi{}^{\mathrm{I}}+A_\pi{}^{\mathrm{II}}. \quad (22)$$

We can take advantage of two factors peculiar to $CuCl_2\cdot 2H_2O$ to resolve the uncertainty in the sign of the hyperfine field below T_N. The two factors are, the disparity between the bond I and bond II lengths and the highly anisotropic hyperfine field at the Cl nuclei.

[32] M. Tinkham, Proc. Roy. Soc. (London) **A236**, 549 (1956).

If the upper sign is correct in the last two relations in Eqs. (19) [i.e., $(A^{\mathrm{I}}-A^{\mathrm{II}})_{\xi}>0$] then (units are $10^{-4}\mathrm{cm}^{-1}$),

$$A_\xi{}^{\mathrm{II}}=0.0\pm 0.7,$$
$$A_\zeta{}^{\mathrm{II}}=0.4\pm 0.6(1.7\pm 0.6),$$
$$A_\xi{}^{\mathrm{I}}=17.7\pm 0.7,$$

and

$$A_\zeta{}^{\mathrm{I}}=2.5\pm 0.6(1.0\pm 0.6). \quad (23)$$

However, if the lower sign choice is correct [i.e., $(A^{\mathrm{I}}-A^{\mathrm{II}})_{\xi}<0$] the I and II bond contributions in Eq. (23) are exchanged. This would mean that the contribution from bond I to $(A^{\mathrm{I}}+A^{\mathrm{II}})_{\xi}$ would be negligible. Therefore, the upper sign must be selected. With the selection of one of two possible sets of values (for a given θ_{int}) for the hyperfine field below T_N, Eq. (19) can be considered as representing the results of five distinct measurements. If we combine the numerical values in Eq. (19) with Eq. (22) the results for case (a) are (units are 10^{-4} cm^{-1}),

$$A_s{}^{\mathrm{I}}+A_s{}^{\mathrm{II}}=7.8\pm 0.6,$$
$$A_s{}^{\mathrm{I}}-A_\pi{}^{\mathrm{I}}=7.6\pm 0.6(6.6\pm 0.6),$$
$$A_\sigma{}^{\mathrm{I}}=5.1\pm 0.5(5.6\pm 0.5),$$
$$A_s{}^{\mathrm{II}}-A_\pi{}^{\mathrm{II}}=0.1\pm 0.5(0.6\pm 0.5),$$

and

$$A_\sigma{}^{\mathrm{II}}=0.1\pm 0.5(0.6\pm 0.5). \quad (24)$$

Only the values for the total isotropic contribution, $A_s{}^{\mathrm{I}}+A_s{}^{\mathrm{II}}$, and $A_\sigma{}^{\mathrm{I}}$, should be considered as significant.

We can conclude from the results listed in Eq. (24) that the hyperfine field is dominated by the bond I s and p_σ contributions. The p_π contribution is negligible for $\theta_{\mathrm{int}}\cong 32°$ but the sum of the terms $A_s{}^{\mathrm{II}}+A_\pi{}^{\mathrm{I}}$ is greater than the experimental uncertainty for $\theta_{\mathrm{int}}\cong 40°$. The bond II contribution is negligible except for the value of $A_\zeta{}^{\mathrm{II}}$ for $\theta_{\mathrm{int}}\cong 40°$. It is clear from these results that we cannot choose between the two possible orientations of H_{int} below T_N.

B. Case (b)

If the $\alpha(1)$ transition in Fig. 4 is associated with a Cl(2) site rather than a Cl(1) site, the principal axis system of $\{\Delta H/H_0\}$ at a Cl(1) site is oriented as shown in Fig. 5 (b). The method we use to analyze the hyperfine data in case (b) is identical to that followed in case (a). The only result that differs significantly from the case (a) values is,

$$A_\sigma{}^{\mathrm{I}}\cong -5.6\times 10^{-4}\ \mathrm{cm}^{-1}. \quad (25)$$

Since $A_\sigma{}^{\mathrm{I}}$ represents the difference between the $p_\sigma{}^{\mathrm{I}}$ and $p_{\pi'}{}^{\mathrm{I}}$ contributions to the hyperfine field, a large negative value for $A_\sigma{}^{\mathrm{I}}$ indicates that the anisotropic part of the hyperfine field is dominated by $p_{\pi'}$ interactions in the ac plane.

The lowest state of a free Cu^{++} ion is the ^2D state which corresponds to a single hole in an otherwise

closed $3d$ valence shell. The one-electron eigenfunctions for the Cu^{++} ion in a crystal field appropriate to $CuCl_2\cdot 2H_2O$ have been determined by Nagamiya, Yosida, and Kubo[33] for the case of a single ^2D configuration. While no experimental crystal-field data are available for $CuCl_2\cdot 2H_2O$, it is generally assumed[34] that the Cu Tutton salts offer a reasonable facsimile of the Cu^{++} environment in $CuCl_2\cdot 2H_2O$. In the case of the Cu Tutton salts, the ground-state manifold consists of two orbital singlets (Kramers doublets) split by spin-orbit coupling and the noncubic part of the crystal field. These states consist primarily of admixtures of the two $d\gamma$ states (x^2-y^2, $3z^2-r^2$). The excited-state manifold consists of three orbital singlets (Kramers doublets) roughly 10^4 cm^{-1} above the ground state. The excited states are primarily admixtures of the three $d\epsilon$ states (xy,xz,yz). To the extent that the comparison between the Cu^{++} environment in the Tutton salts and $CuCl_2\cdot 2H_2O$ is valid, it follows that the three excited state orbital singlets in $CuCl_2\cdot 2H_2O$ contain most of the $d\epsilon$ contribution and the single unpaired Cu^{++} spin is in an orbital which is predominantly $d\gamma$. In a cubic field the π contribution to the transferred hyperfine field results from interactions between the ligand p_π and $p_{\pi'}$ electrons and the $d\epsilon$ orbitals. We conclude that the p_σ contribution to the transferred hyperfine field in $CuCl_2\cdot 2H_2O$ should be greater than the p_π contribution and that the assignment illustrated in Fig. 5(a) is correct.

The results of the calculations of the EFG discussed in Sec. VI are also consistent with the choice of case (a) over case (b). In all three of the calculations, the smallest of the principal values of the EFG corresponds to a direction lying near bond II. In case (b) the maximum principal value of the EFG is roughly 16° from the bond II direction.

VIII. SUMMARY AND DISCUSSION

We have determined the orientations and principal values of the EFG and hyperfine field at a Cl nucleus in $CuCl_2\cdot 2H_2O$. The orientation of the EFG is in better agreement with point-charge-model predictions than with the results of the calculation of Rao and Narasimhamurty[16] in which induced electric-dipole contributions were included. The Cl NMR measurements in the paramagnetic region were consistent with an internal magnetic field whose anisotropic contributions are describable in terms of a symmetric second-rank tensor. The hyperfine field is determined almost solely by s and p_σ contributions associated with the interaction between the Cl^- valence electrons and the $3d$ electrons of the nearest-neighbor Cu^{++} ion.

The values we determine for the hyperfine field parameters at a Cl nucleus in $CuCl_2\cdot 2H_2O$ are in reasonably good agreement with the values for A_s and A_σ determined by Thornley *et al.*[35] in EPR measurements on Cu^{++} spins in $(CuCl_6)^{4-}$ complexes present in mixed crystals of $Cu:CdCl_2$. In addition, a comparison can be made between the hyperfine field at a chlorine nucleus in $CuCl_2\cdot 2H_2O$ and the field at a fluorine nucleus[36] in $CuF_2\cdot 2H_2O$. The structure of $CuF_2\cdot 2H_2O$ is isomorphous to that of $CoCl_2\cdot 2H_2O$ and both fluorine sites in the unit cell are equivalent. Hence, the analysis of the F NMR in $CuF_2\cdot 2H_2O$ is not subject to the ambiguity that was associated with the presence of the two distinguishable Cl sites in $CuCl_2\cdot 2H_2O$. The bond I (1.89 Å) and bond II (2.47 Å) lengths in $CuF_2\cdot 2H_2O$ differ by about 30% as in the case of $CuCl_2\cdot 2H_2O$. Thus, the nearest-neighbor configuration in $CuF_2\cdot 2H_2O$ is essentially like that in $CuCl_2\cdot 2H_2O$. Shulman and Wyluda neglected the bond II contribution and associated the total anisotropic hyperfine field with p_σ interactions. They found $A_s=(86\pm 6)\times 10^{-4}$ cm^{-1} and $A_\sigma=(24\pm 5)\times 10^{-4}$ cm^{-1} (at a ^{19}F nucleus), with the p_σ axis lying along the bond I direction. This result is consistent only with our case (a). If we assume with Shulman and Wyluda that the bond II contributions to the hyperfine field are negligible, then we find (units are 10^{-4} cm^{-1})

$$A_s^{\mathrm{I}}=7.8\pm 0.6,$$
$$A_\sigma^{\mathrm{I}}=5.0\pm 0.7,$$
and
$$A_\pi^{\mathrm{I}}=0.0\pm 0.7, \qquad (26)$$

at a ^{35}Cl nucleus in $CuCl_2\cdot 2H_2O$. These values agree to within experimental error with the results in Eq. (24) for $\theta_{\mathrm{int}}\cong 32°$.

TABLE II. The transferred hyperfine-field single-bond components in kOe for $CuF_2\cdot 2H_2O$, $CuCl_2\cdot 2H_2O$, and $(CuCl_6)^{4-}$. We use the values listed in Eq. (26) for $CuCl_2\cdot 2H_2O$. The numbers in brackets along side the $CuF_2\cdot 2H_2O$ A_s and A_σ values are the respective fractional $2s$ and $2p$ unpaired spin densities in %.

	Nearest-neighbor separation (Å)	A_s (kOe)	A_σ (kOe)
$CuCl_2\cdot 2H_2O$	2.27	28	18
$(CuCl_6)^{4-}$		34	16
$CuF_2\cdot 2H_2O$	1.89	32[0.5]	9[5.5]

In Table II we list the effective s and p contributions to the transferred hyperfine field in $CuCl_2\cdot 2H_2O$, $CuF_2\cdot 2H_2O$ and $(CuCl_6)^{4-}$ complexes in $CdCl_2$. The effective s contributions to the hyperfine field in $CuCl_2\cdot 2H_2O$ and $CuF_2\cdot 2H_2O$ agree to within experimental error. However, it is significant that the value for A_σ in $CuCl_2\cdot 2H_2O$ [and $(CuCl_6)^{4-}$] is roughly twice that in $CuF_2\cdot 2H_2O$. If we assume that only the chlorine $3p$ electrons contribute to A_σ in $CuCl_2\cdot 2H_2O$ then the

[33] T. Nagamiya, K. Yosida, and R. Kubo, *Advances in Physics* (Taylor & Francis Ltd., London, 1955), Vol. 4, p. 1.
[34] T. Nagamiya, Progr. Theoret. Phys. (Kyoto) **11**, 309 (1954).
[35] J. H. M. Thornley, B. W. Mangum, J. H. E. Griffiths, and J. Owen, Proc. Phys. Soc. (London) **78**, 1263 (1961).
[36] R. G. Shulman and B. J. Wyluda, J. Chem. Phys. **35**, 1498 (1961).

degree of $3p$ electron unpairing is roughly,

$$f_{3p}=A_\sigma/A_{3p}. \quad (27)$$

The atomic hyperfine constant A_{3p} in Eq. (26) has the expectation value,

$$A_{3p}=\tfrac{4}{5}\pi\mu_B\gamma_N\hbar\langle 1/r^3\rangle_{3p}=0.00488\ \text{cm}^{-1}, \quad (28)$$

where the factor $\langle 1/r^3\rangle_{3p}$ is determined from the paper of Barnes and Smith.[37] The resultant fractional unpairing is, $f_{3p}=0.10$ which is approximately twice the value estimated by Shulman and Wyluda for f_{2p} in $CuF_2\cdot 2H_2O$. However, the estimate of f_{3p} for $CuCl_2\cdot 2H_2O$ may be sharply reduced by the contributions to A_σ of the Cl $2p$ electrons.

[37] R. G. Barnes and W. V. Smith, Phys. Rev. **93**, 95 (1954).

ACKNOWLEDGMENT

We would like to acknowledge many helpful discussions with Dr. A. Narath.

PHYSICAL REVIEW VOLUME 140, NUMBER 5A 29 NOVEMBER 1965

Influence of the Peierls Potentials on the Reversible Stress-Strain Relation for Dislocations

G. ALEFELD, R. H. CHAMBERS, AND T. E. FIRLE
General Atomic Division of General Dynamics Corporation, John Jay Hopkins Laboratory for Pure and Applied Science, San Diego, California

The mechanical equation of state of kinked dislocations is considered. Contrary to dislocation strings, which follow under the assumption of constant line tension a linear stress-strain relation for stresses $\sigma/G<b/3L$ (L=line length, b=Burgers vector, G=shear modulus, σ=stress), one finds significant nonlinearities in the reversible stress-strain relation of kinked dislocations. The physical reason for the nonlinearities can be ascribed to the fact that, owing to the Peierls potentials, the energy of a dislocation increases in multiples of the double-kink energy $2W_k$ (W_k=kink energy). A linear range, which is confined to stresses $\sigma/G<(10^{-1}b/L)(\sin\varphi+5kT/Gb^3)$ (φ=angle against close-packed direction, T=temperature), is followed by a region with $\partial^2\epsilon/\partial\sigma^2<0$ (ϵ=strain). This region corresponds to the restricted motion of geometrical kinks. After passing through an inflection point, which is roughly determined by $\sigma/G=\alpha(b/L)(2W_k/Gb^3)$ (α=numerical factor between 1 and 2), a region with $\partial^2\epsilon/\partial\sigma^2>0$ follows. It is caused by double-kink generation. If the measuring time is too short for thermally activated double kink generation, the inflection point is determined by the stress which is required for stress-assisted thermally activated double kink generation. At $T=0$°K, the stress of the inflection point provides a measure for the Peierls stress. It is suggested that evidence for the Peierls potentials can be established through a verification of the nonlinear-stress-strain relation by the following experiments: (a) The restricted motion of geometric kinks should be detectable beyond the stress for activating Frank-Read sources as a *decrease* of the modulus defect with increasing stress amplitude. (b) The double-kink-generation peaks should, in *undeformed* material, rise out of the background in high-amplitude measurements. (c) The double-kink-generation peaks should be found in *undeformed* pure material by applying a static-bias stress. (d) In deformed material, high-amplitude oscillations should cause an increase of the peak height before the peak starts to shift to lower temperatures.

I. INTRODUCTION

THIS paper seeks to point out that the reversible stress-strain relation of bowing dislocation segments, as a direct consequence of the Peierls potentials, differs in a very characteristic manner from that of dislocation segments in a material with vanishing Peierls potentials. The Peierls potentials cause the stress-strain relation to become intrinsically nonlinear at relatively small stresses.[1] Consequently, the Peierls stress will be the source of amplitude-dependent internal friction and modulus defect.[1] A verification of the experimental consequences predicted by the particular stress-strain relation can be considered evidence for a finite Peierls stress and will also allow the Peierls stress to be measured directly.

Depending on the geometric kink density, one can divide the problem of deriving the equation of state of a kinked dislocation as follows: For low kink density (=low geometric kink density and not too high temperatures) the interaction of kinks can be ignored and the strain as a function of stress is determined by entropy changes of the kinks. The thermodynamic treatment follows closely the analogy to a one-dimensional gas. For high geometric kink density the change of the interaction of the kinks with stress dominates over entropy changes. Consequently, the stress-strain relation is determined by the interaction law of kinks. Between these two extremes extends a range in density for which the thermodynamic problem is very similar to that of real gases. A rigorous derivation of the stress-strain relation, including double-kink generation, is only possible for noninteracting kinks (Sec. II).

[1] G. Alefeld, J. Appl. Phys. **36**, 2642 (1965).